Dynamic Weight Adaptation in Spiking Neural Networks Inspired by Biological Homeostasis

Yunduo Zhou[1], Bo Dong[2], Chang Li[1], Yuanchen Wang[1], Xuefeng Yin[1], Yang Wang[1], Xin Yang[1]*

[1]Key Laboratory of Social Computing and Cognitive Intelligence, Dalian University of Technology
[2]Cephia AI
zyd_dlut@163.com, bo.dong@cephia.ai, lchang@mail.dlut.edu.cn, wangyc0604@mail.dlut.edu.cn, xfyin@mail.dlut.edu.cn, yangwang06@mail.dlut.edu.cn, xinyang@dlut.edu.cn

Abstract

Homeostatic mechanisms play a crucial role in maintaining optimal functionality within the neural circuits of the brain. By regulating physiological and biochemical processes, these mechanisms ensure the stability of an organism's internal environment, enabling it to better adapt to external changes. Among these mechanisms, the Bienenstock, Cooper, and Munro (BCM) theory has been extensively studied as a key principle for maintaining the balance of synaptic strengths in biological systems. Despite the extensive development of spiking neural networks (SNNs) as a model for bionic neural networks, no prior work in the machine learning community has integrated biologically plausible BCM formulations into SNNs to provide homeostasis. In this study, we propose a Dynamic Weight Adaptation Mechanism (DWAM) for SNNs, inspired by the BCM theory. DWAM can be integrated into the host SNN, dynamically adjusting network weights in real time to regulate neuronal activity, providing homeostasis to the host SNN without any fine-tuning. We validated our method through dynamic obstacle avoidance and continuous control tasks under both normal and specifically designed degraded conditions. Experimental results demonstrate that DWAM not only enhances the performance of SNNs without existing homeostatic mechanisms under various degraded conditions but also further improves the performance of SNNs that already incorporate homeostatic mechanisms.

Code — https://github.com/Zyunduo/AAAI_2026_DWAM

1 Introduction

Homeostasis in biological organisms is a critical mechanism for maintaining survival and functionality by regulating physiological and biochemical processes to ensure internal environmental stability (Marder and Goaillard 2006; Desai 2003; Turrigiano and Nelson 2004; Marder and Prinz 2002; Mease et al. 2013). In the nervous system, homeostasis can be achieved through various mechanisms such as synaptic scaling, excitatory-inhibitory balance, Bienenstock, Cooper, and Munro (BCM) theory, and dynamic firing thresholds (Desai 2003; Keck, Hübener, and Bonhoeffer 2017; Turrigiano and Nelson 2004). These mechanisms finely tune and balance neuronal activity, ensuring that the nervous system maintains a relatively stable activity level in response to external stimuli or internal disturbances, thereby preventing excessive excitation or inhibition of neurons. Several studies have shown that the absence or dysregulation of neuronal homeostasis can cause neuronal activity levels to escalate rapidly, resulting in network dysfunction (O'Leary et al. 2014; Marder and Prinz 2002).

Given the critical role of homeostasis in biological neural networks, many researchers have sought to incorporate this mechanism into spiking neural networks (SNNs) to enhance networks' performance (Meng, Jin, and Yin 2011; Hao et al. 2020; Kim et al. 2021; Xu, Liu, and Pei 2022; Hao et al. 2021). Due to the bio-inspired nature of SNNs, incorporating biological mechanisms into them is relatively straightforward (Roy, Jaiswal, and Panda 2019; Maass 1997), making SNNs an ideal platform for such endeavors. However, while previous attempts have introduced homeostatic mechanisms into SNNs, most of these approaches have been heuristic or empirical, lacking biological interpretability and failing to validate the effectiveness of neural homeostasis in artificial systems. Ding et al. (Ding et al. 2022) addressed this gap by proposing a biologically plausible method to implement homeostasis in SNNs through dynamic firing thresholds. Inspired by the adaptive thresholding observed in barn owl cochlear neurons, their method calculates the firing threshold of each neuron in real time based on membrane potential, dynamically modulating neuronal activity levels. This approach successfully introduces homeostasis into SNNs by regulating intrinsic neuronal properties.

Nonetheless, achieving homeostasis solely by adjusting intrinsic neuronal properties is incomplete. In biological systems, homeostasis depends not only on the regulation of individual neurons but also on the dynamic balance of interneuronal relationships (Desai 2003; Keck, Hübener, and Bonhoeffer 2017). The BCM theory (Bienenstock, Cooper, and Munro 1982), a classical model of synaptic plasticity, is a key mechanism for maintaining homeostasis by adapting synaptic weights based on neurons' historical activity levels to stabilize subsequent neuronal responses. Based on this theory, we developed the Dynamic Weight Adaptation Mechanism (DWAM), a mechanism that dynamically adjusts network weights in real-time according to the firing relationships and activity levels of neurons. Specifically,

*Corresponding author.

DWAM provides two key contributions: 1) It assesses firing relationships between neurons to evaluate their correlation, enhancing weights between highly correlated neurons while weakening those between weakly correlated ones, thereby maintaining accurate inter-neuronal associations. 2) It dynamically determines the direction of weight modifications based on neuronal activity levels, preventing sustained enhancement of highly correlated neurons or persistent weakening of weakly correlated neurons, ensuring long-term balance and network stability.

While DWAM is inspired by the BCM theory, maintaining consistency with its principles and formulaic structure, the inherent differences between SNNs and biological neural systems make the direct application of the original biological BCM model ineffective for introducing homeostasis into SNNs. Therefore, we analyze the original BCM model and leverage the statistical firing patterns of SNN neurons to refine the strength of weight adjustments, tailoring it for application in SNNs.

We validated our method through dynamic obstacle avoidance and continuous control tasks under both normal and specifically designed degraded conditions. Across all scenarios, the developed BCM mechanism consistently delivered performance improvements. Notably, these gains were achieved by directly integrating DWAM into the host SNNs, without any fine-tuning.

In particular, we make the following contributions in this work:

- We propose a dynamic weight adaptation mechanism for SNNs, which represents the first implementation of biologically inspired homeostasis from the perspective of inter-neuronal relationships, based on the BCM theory.
- We design an approach that optimizes the original biological model's weight adjustment strength using statistical firing cues from neurons, ensuring higher stability and feasibility in SNNs.
- We validate the effectiveness of the proposed method across multiple tasks and degraded conditions, demonstrating that DWAM achieves biologically inspired homeostasis and significantly enhances SNN generalization across diverse tasks and conditions. Notably, all results are obtained by directly integrating DWAM into host SNNs without any fine-tuning, highlighting its plug-and-play nature.

2 Background and Related Work

2.1 Homeostasis and BCM Theory

The BCM theory provides a framework for understanding synaptic plasticity by describing how synaptic weights change in response to neuronal activity. According to BCM theory, the synaptic modification is governed by the rule (Bienenstock, Cooper, and Munro 1982):

$$\frac{dw_{ij}}{dt} = \phi(x_i)x_j \tag{1}$$

$$\phi(x_i) = x_i(x_i - \theta_M) \tag{2}$$

where w_{ij} is the synaptic weight of the connection between neuron i and neuron j, x_j is the presynaptic activity, x_i is the postsynaptic activity, and $\phi(x_i)$ is a function of the postsynaptic activity. Here, θ_M is a sliding modification threshold that adapts based on the history of postsynaptic activity and ensures a balance between synaptic potentiation (when $x_i > \theta_M$) and depression (when $x_i < \theta_M$). The sliding modification threshold θ_M is typically given by:

$$\theta_M = \left\langle x_i^2 \right\rangle \tag{3}$$

where $\left\langle x_i^2 \right\rangle$ represents the long-term average of the squared postsynaptic activity.

2.2 Spiking Neural Networks (SNNs)

SNNs are a class of biologically inspired neural networks that aim to replicate the information processing mechanisms of biological neurons. Unlike traditional networks that process continuous signals, SNNs transmit information through discrete spikes, which occur when a neuron's membrane potential exceeds a certain threshold. These spikes are generated by the integration of incoming signals over time. When the potential reaches the threshold, the neuron "fires", sending a spike to neighboring neurons, and the potential resets.

Over the years, various neuron models have been developed to simulate the dynamics of spiking neurons, with two commonly used ones being the Spike Response Model (SRM) (Gerstner 1995) and the Leaky Integrate-and-Fire (LIF) model (Gerstner and Kistler 2002). More details about these two models are provided in Supplementary Note 2.

2.3 SNN with Homeostasis

Although homeostatic mechanisms are well studied in biology, their integration in machine learning is limited. Some works adopt BCM or STDP to guide SNN learning (Meng, Jin, and Yin 2011; Pan et al. 2023; Kheradpisheh et al. 2018; Gupta and Saurabh 2024; Wang et al. 2024), but they are task-specific or applied only during training, offering no functional homeostasis during inference and thus not directly comparable to our approach.

Other works have attempted to introduce homeostatic effects during the testing phase by adapting neuronal parameters such as thresholds or synaptic strengths (Hao et al. 2020; Kim et al. 2021; Xu, Liu, and Pei 2022; Zhang et al. 2025, 2022; Wang et al. 2023). However, these approaches are largely empirical or heuristic in nature, lacking biological interpretability and principled justification.

In contrast, Ding et al. (Ding et al. 2022) proposed a biologically inspired method for calculating the dynamic membrane potential threshold in SNNs. This threshold is related to the neuron's membrane potential and the previous depolarization rate. They also demonstrated the advantages of their method compared to the aforementioned approaches that lack biological grounding. Therefore, the primary comparison method in this study is that of Ding et al.

3 Method

The core concept of the biological BCM theory can be divided into two main components, which describe the mechanism of synaptic strength adjustment and the mechanism for maintaining stability.

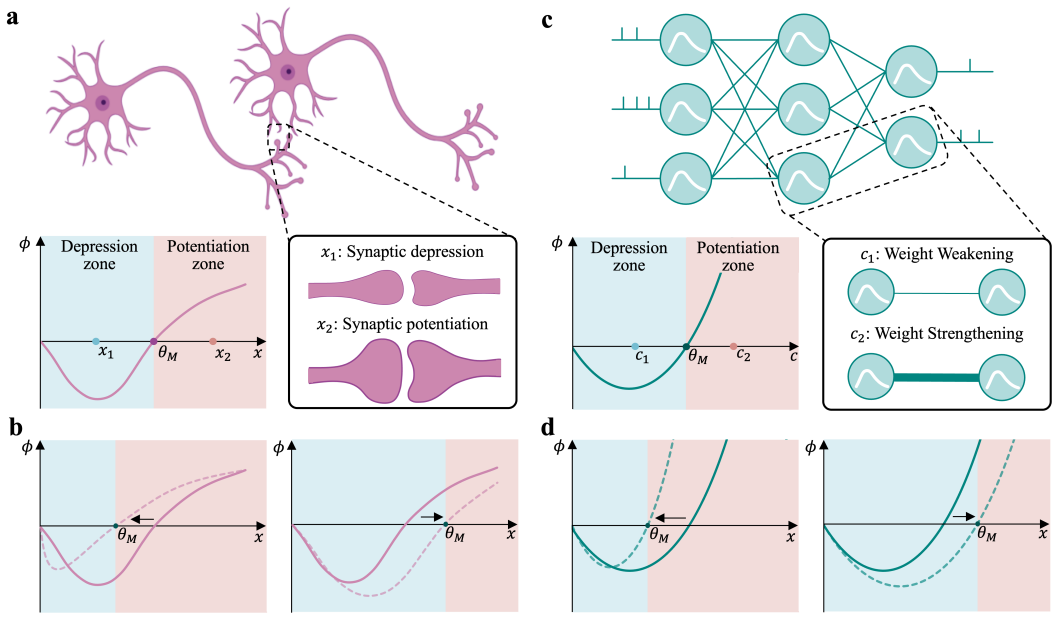

Figure 1: **Comparison between biological BCM theory and the proposed DWAM in SNNs.** a. Illustration of the BCM theory in biological neural systems. The synaptic modification function (ϕ) is governed by the postsynaptic neuron's activity (x) and a modification threshold (θ_M). The depression zone ($x < \theta_M$) leads to synaptic weakening (e.g., x_1), while the potentiation zone ($x > \theta_M$) results in synaptic strengthening (e.g., x_2). b. The dynamic adjustment of the modification threshold (θ_M) based on the historical activity level of the postsynaptic neuron. A higher historical activity level shifts θ_M to the right, reducing potentiation likelihood, whereas lower historical activity shifts θ_M to the left, increasing potentiation likelihood.(illustrated as a shift from the solid line to the dashed line in the figure) c. Proposed DWAM for SNNs, inspired by the BCM theory. The synaptic modification function (ϕ) in DWAM operates on a similar principle, where the postsynaptic neuron's firing rate (c) interacts with a modification threshold (θ_M) to determine weight weakening (c_1) or strengthening (c_2). d. As with BCM, a higher historical firing rate shifts θ_M to the right, whereas a lower firing rate shifts it to the left, enabling balanced and stable weight updates in the SNNs.

The first component describes how synaptic strength is adjusted based on the postsynaptic neuron's activity relative to a modification threshold. As shown in Figure 1a, when the presynaptic neuron fires and the postsynaptic activity (e.g., x_1) is below the threshold (θ_M), the synapse is considered weakly correlated and is suppressed. Conversely, when the activity (e.g., x_2) exceeds θ_M, the synapse is strengthened. This mechanism dynamically modulates synaptic strength according to neuronal correlation, promoting balanced synaptic regulation.

The second component governs the dynamic adaptation of the modification threshold itself based on the postsynaptic neuron's activity history (Figure 1b). Low historical activity lowers θ_M, increasing the chance of synaptic strengthening, while high activity raises θ_M, promoting synaptic weakening. This prevents unbounded potentiation or depression, maintaining synaptic stability over time.

In this study, we incorporate the BCM theory into SNNs to achieve a biologically inspired homeostatic mechanism. While prior work such as BDETT (Ding et al. 2022) introduces homeostasis by regulating intrinsic neuronal properties during training, our approach focuses on inter-neuronal relationships, providing a complementary and orthogonal mechanism that can coexist with intrinsic regulation. Importantly, unlike BDETT which requires retraining to exploit noise resilience, our method is plug-and-play and can be applied directly to pre-trained SNNs during inference, enabling homeostasis without extra computational cost. This combination of biological plausibility, orthogonal homeostatic strategy, and deployment efficiency makes our approach both practically and conceptually significant.

Section 3.1 elaborates on how to implement the synaptic strength adjustment mechanism in SNNs, corresponding to the first component of the BCM theory. Section 3.2 introduces the realization of the stability maintenance mechanism in SNNs, addressing related challenges and presenting our solutions. Together, these two components form the proposed DWAM.

3.1 The Synaptic Adjustment Mechanism

The synaptic strength adjustment mechanism in SNNs can be implemented by substituting the firing rate c of spiking neurons for the activity level x of biological neurons in Eqs. 1 and 2. At a given timestamp t, the modification of

the weight from the j-th neuron in the $l-1$-th layer to the i-th neuron in the l-th layer is defined as follows:

$$w_{ij}(t) = w_{ij}(t-1) + \phi_{ij}(t) c_j^{l-1}(t) |w_{ij}(t-1)| \psi, \quad (4)$$

$$\phi_{ij}(t) = c_i^l(t) \left(c_i^l(t) - \theta_i^l(t) \right) \quad (5)$$

where ϕ is the modification function for the weights; c is the firing rate of the neuron; θ is the sliding modification threshold; w_{ij} is the weight from the j-th neuron in the $l-1$-th layer to the i-th neuron in the l-th layer, and ψ is a constant. In this implementation, we employ $|w|\psi$ as a scaling factor to dynamically adjust the magnitude of weight changes based on the current weight value. This design ensures that the adjustment for smaller weights does not become excessively large, preventing undue disruption to their stability. Similarly, it allows larger weights to receive sufficient adjustments, avoiding under-scaling that could reduce the effectiveness of weight modulation.

According to these formulas, the weight change is proportional to the product of the modification function and the presynaptic neuron firing rate. Additionally, the postsynaptic neuron firing rate is governed by a dynamic threshold level (θ). When the current firing rate exceeds this threshold, the weight is strengthened; conversely, when the firing rate falls below the threshold, the weight is weakened. As shown in Figure 1c, this process aligns with the first component of the biological BCM theory.

3.2 The Stability Maintenance Mechanism

According to the BCM theory, the sliding modification threshold θ_M in Eq.3 is a super-linear function of the history of postsynaptic activity. Benuskova et al. (Benuskova, Diamond, and Ebner 1994) developed a computational model of a single representative barrel cell based on the BCM theory, where θ_M is defined as:

$$\theta_M(t) = \left[\frac{\langle c^2(t) \rangle_\tau}{\eta} \right], \quad (6)$$

$$\langle c^2(t) \rangle_\tau = \frac{1}{\tau} \int_{-\infty}^{t} c^2(t') e^{-\frac{(t-t')}{\tau}} dt' \quad (7)$$

where η and τ are positive scaling constants. From these relations, it follows that $\theta_M(t)$ is positively correlated with the past firing rate, and thus it can be used to measure the averaged neuron activity in the recent past. To make it applicable to SNNs, we discretize Eqs. 6 and 7 as:

$$\theta_{M,i}^l(t) = (1-\alpha)\theta_{M,i}^l(t-1) + \alpha (c_i^l(t))^2 \quad (8)$$

This is a commonly used recursive form of exponential moving average, where α controls the update rate and corresponds to the decay constant of the sliding modification threshold.

Although Eqs. 4, 5, and 8 successfully reproduce the BCM theory in biological neural systems, when θ_M defined in Eq. 8 is used as $\theta_i^l(t)$ in Eq. 5, the resulting SNN applying Eqs. 4, 5, and 8 fails to achieve the expected performance. To distinguish this approach from the final method, we refer to the method based on these three equations as Biological-Originated DWAM (BioDWAM). This discrepancy arises primarily due to differences in neuronal firing rates. In biological systems, neurons typically maintain relatively low firing rates to ensure sparse coding and energy efficiency (Olshausen and Field 1996; Stringer et al. 2019). However, in SNNs, some neurons may need to sustain high firing rates for extended periods to meet task requirements and maintain network performance. When a neuron exhibits prolonged high firing rates, the sliding modification threshold gradually increases and stabilizes at a high level. According to Eqs. 4 and 5, this leads to continuous weakening of the weights connected to the neuron, preventing the network from reaching a stable state.

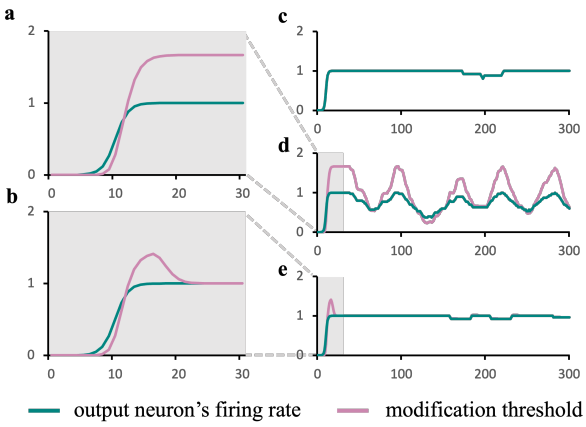

Figure 2: **Behavioral comparison between BioDWAM and DWAM in the toy example.** All subplots show simulation steps (x-axis) versus value (y-axis), with green and pink curves indicating firing rate and modification threshold, respectively. a & b. Zoomed-in views of the initial phase in d and e, showing early threshold adaptation. c. Firing rate stabilizes at 1 without synaptic adjustment. d. BioDWAM induces oscillatory instability at high firing rates. e. DWAM maintains stability by modulating threshold according to firing variability.

To illustrate this phenomenon, we designed a toy example. In this setup, the output layer of the network contains only a single neuron, trained to maintain a high firing rate, ideally close to 1. We applied BioDWAM directly to the output layer of this network and recorded the changes in the output neuron's firing rate and modification threshold over time. See Supplementary Note 3 for further training details.

Figure 2c shows the firing rate of the output neuron without the application of BioDWAM. The firing rate gradually increases and stabilizes at 1, representing the ideal behavior of the network. In contrast, Figure 2d illustrates the behavior when BioDWAM is applied. Initially, when the output neuron's firing rate is low, the sliding modification threshold remains within a reasonable range. However, as the firing rate increases to a high level, the threshold rises significantly. According to Eqs. 4 and 5, this results in a weakening of the

weights connected to the neuron. As a consequence, the firing rate begins to decrease. Once the firing rate falls below the sliding modification threshold, the weights are strengthened again, causing the firing rate to rise once more. This cycle continues, leading to an unstable oscillatory output characterized by wave-like patterns.

This observation highlights that directly applying the original biological synaptic adjustment model to SNNs can introduce stability issues, particularly when dealing with neurons with high firing rates.

Our Solution To retain the original stabilizing effect of the BCM theory in neural networks and to avoid the instability caused by high firing-rate neurons, we introduce a balancing term in Eq. 8:

$$\theta_i^l(t) = \theta_{M,i}^l(t)\zeta\frac{\sigma(c_i^l, n)}{\mu(c_i^l, n)} + c_i^l(t)(1 - \zeta\frac{\sigma(c_i^l, n)}{\mu(c_i^l, n)}) \quad (9)$$

Here, ζ is a positive scaling constant, and σ and μ denote the standard deviation and mean of the postsynaptic neuron's firing rates over the past n time steps. Their ratio, $\frac{\sigma}{\mu}$, is the coefficient of variation (CV), which reflects the stability of neuronal activity.

As shown in Eq.9, the CV modulates the influence of the biologically originated sliding threshold $\theta_{M,i}^l(t)$ on $\theta_i^l(t)$. A high CV (i.e., unstable firing) increases the influence of $\theta_{M,i}^l(t)$, pulling $\theta_i^l(t)$ toward it. Conversely, a low CV (i.e., stable firing) causes $\theta_i^l(t)$ to align more closely with the current firing rate. As indicated in Eqs.4 and 5, when $\theta_i^l(t)$ matches the firing rate, weight updates diminish, preventing persistent high-frequency firing from continuously weakening synaptic weights.

We applied DWAM to the same toy example as before. As shown in Figure 2e, DWAM effectively mitigates the instability observed in BioDWAM at high firing rates. To better illustrate the behavioral differences, the early phases of Figure 2d and e are enlarged in Figure 2a and b. Initially, DWAM behaves similarly to BioDWAM, but once the neuron stabilizes at a high firing rate, DWAM's correction threshold gradually converges to that rate. This allows DWAM to retain the biologically consistent behavior of the BCM theory at low firing rates while avoiding the instability seen when directly applying the biological model to SNNs.

By integrating Eqs. 4, 5, and 9, we successfully incorporate the BCM theory into SNNs, providing biologically-plausible homeostasis for the network.

4 Experiments and Results

We validated the effectiveness of DWAM in two types of tasks: a robot obstacle avoidance task and continuous control tasks. To further evaluate its generalization across different neuron models, we conducted experiments using both LIF and SRM neurons.

Robotic Obstacle Avoidance Task: In this task, the robot navigates from a random start to a target point in an obstacle-filled environment. A trial is successful if the robot reaches the target without collisions. Each round includes 200 trials, with the success rate (SR) defined as: $\text{SR} = \frac{N_{\text{success}}}{N_{\text{total}}}$, where N_{success} is the number of successful trials and $N_{\text{total}} = 200$. The task is repeated over five rounds, and the final evaluation metric is the average success rate across all rounds.

Continuous Control Tasks: We used two standard OpenAI Gym environments (Brockman 2016): HalfCheetah-v3 and Ant-v3. The goal is to control a half-mechanical cheetah or a quadruped robot to move forward over 1000 steps while maximizing forward velocity. Each round consists of 10 trials, and the highest cumulative reward is recorded per round. The task is repeated for 10 rounds, and the average score across rounds is used for evaluation.

In addition to performance metrics (SR and reward), we evaluated the homeostasis of host SNNs using two firing-rate-based measures: HM_m and HM_{std}. These measures quantify the mean and variance of absolute changes in neuron firing rates across P degraded-condition trials, relative to the standard condition, reflecting the stability of network activity. Details on these measures can be found in Supplementary Note 4.

Experimental Setup Robotic Obstacle Avoidance Task: We selected two types of host SNNs: one without a homeostasis mechanism, the Spiking Action Network (SAN) (Tang, Kumar, and Michmizos 2020), and another with the best current homeostasis mechanism, the Bioinspired Dynamic Energy-Temporal Threshold (BDETT) (Ding et al. 2022). SAN and BDETT were first trained using the spiking deep deterministic policy gradient (SDDPG) framework (Tang, Kumar, and Michmizos 2020). After training, we directly integrated DWAM into the trained models without any further retraining, resulting in SAN-DWAM and BDETT-DWAM. We then conducted comparisons within each model group (i.e., SAN vs. SAN-DWAM, and BDETT vs. BDETT-DWAM) to evaluate the effectiveness of DWAM. See Supplementary Note 5 for further training details.

Continuous Control Task: we selected two types of host SNNs: one without a homeostasis mechanism, the population-coded SAN (PopSAN) (Tang et al. 2020), and the other with the best current homeostasis mechanism, BDETT (Ding et al. 2022). PopSAN is an improved version of SAN, featuring specifically designed encoders and decoders to handle high-dimensional control tasks. We construct PopSAN-DWAM and BDETT-DWAM using the same method as the obstacle avoidance task. Both PopSAN and BDETT were trained using the twin-delayed deep deterministic policy gradient (TD3) algorithm (Fujimoto, Hoof, and Meger 2018). See Supplementary Note 6 for further training details.

To verify the necessity of our modifications to the original biological formulation, we further conducted controlled comparisons by integrating BioDWAM into SAN, PopSAN, and BDETT, resulting in SAN-BioDWAM, PopSAN-BioDWAM, and BDETT-BioDWAM. These variants were included in the experiments as supplementary baselines. Their results and implementation details are provided in Supplementary Notes 5 and 6.

4.1 Robotic Obstacle Avoidance with DWAM

In this task, a mobile robot navigates from a random start to a random target within a given scene, using a Robot Peak light

	0.2				6.0				GN			
	LIF		SRM		LIF		SRM		LIF		SRM	
Name	SR	HM_m/HM_{std}	SR	HM_m/HM_{std}	SR	HM_m/HM_{std}	SR	HM_m/HM_{std}	SR	HM_m/HM_{std}	SR	HM_m/HM_{std}
SAN	88.2%	0.109/0.115	86.0%	0.130/0.117	71.7%	**0.018/0.022**	75.6%	0.027/0.028	87.6%	0.033/0.031	81.6%	0.039/**0.034**
SAN-DWAM	**90.6%**	**0.091/0.113**	**87.3%**	**0.121/0.112**	**84.3%**	**0.018/0.022**	**76.1%**	**0.026/0.027**	**88.4%**	**0.031/0.030**	**83.3%**	**0.037/0.034**
BDETT	70.7%	0.104/0.109	64.0%	0.073/0.097	79.6%	0.016/0.022	71.6%	0.021/**0.022**	87.5%	0.025/**0.026**	73.4%	**0.019**/0.023
BDETT-DWAM	**82.6%**	**0.103/0.103**	**75.0%**	**0.070/0.096**	**82.8%**	**0.015/0.021**	**80.0%**	**0.017/0.022**	**89.3%**	**0.024/0.026**	**76.6%**	**0.019/0.022**

	8-bit Loihi weight				GN weight				30% Zero weight			
	LIF		SRM		LIF		SRM		LIF		SRM	
Name	SR	HM_m/HM_{std}	SR	HM_m/HM_{std}	SR	HM_m/HM_{std}	SR	HM_m/HM_{std}	SR	HM_m/HM_{std}	SR	HM_m/HM_{std}
SAN	85.4%	0.005/0.005	**85.5%**	**0.004/0.003**	55.2%	0.144/0.168	0.0%	0.166/0.158	66.3%	0.102/0.104	5.7%	0.108/0.105
SAN-DWAM	**90.1%**	**0.004/0.003**	84.7%	**0.004**/0.004	**70.4%**	**0.106/0.127**	**0.5%**	**0.162/0.148**	**77.4%**	**0.093/0.102**	**14.0%**	**0.105/0.100**
BDETT	91.1%	**0.003/0.003**	83.3%	0.003/**0.002**	79.6%	0.062/0.081	79.0%	0.043/0.051	56.7%	0.057/0.070	56.0%	0.056/0.066
BDETT-DWAM	**93.8%**	**0.003/0.003**	**86.9%**	**0.002/0.002**	**89.8%**	**0.052/0.073**	**84.4%**	**0.035/0.042**	**78.3%**	**0.046/0.057**	**81.6%**	**0.054/0.059**

Table 1: Quantitative performance of the robotic obstacle avoidance task under degraded conditions, where higher SR indicates better performance, and lower HM_m and HM_{std} values reflect improved homeostasis.

detection and ranging (RPLIDAR) sensor for obstacle detection. To evaluate DWAM's homeostatic capability, we tested it under several degraded conditions based on a static environment: (1) dynamic obstacles, by adding moving objects; (2) degraded input, by disturbing LIDAR data using "0.2", "6.0" and "GN" methods; and (3) weight uncertainty, by perturbing trained weights via "8-bit Loihi", "GN weight" and "30% zero weight." Detailed explanations of these disturbance methods can be found in Supplementary Note 5.

Success Rate Table 1 presents the success rate comparison between the host SNN and the host SNN integrated with DWAM under degraded conditions, evaluated on both LIF and SRM neuron models. The integration of DWAM consistently improves the success rates of the host SNN to varying degrees, except for the SAN model using SRM neurons under the 8-bit Loihi weight condition. Notably, SAN-DWAM demonstrates clear performance gains over SAN, particularly under severe input perturbations such as GN noise with LIF neurons. Similarly, BDETT-DWAM shows a consistent advantage over BDETT, especially under conditions involving significant weight degradation. These results show that DWAM effectively introduces a stability mechanism into SNNs lacking intrinsic homeostasis, enabling them to overcome challenging conditions. The observed improvements also suggest that multiple stability mechanisms can coexist within SNNs, supporting the viability of our approach.

Homeostasis Metrics In biological systems, each neuron has a unique firing rate set point. When a network is in homeostasis, the firing rates of individual neurons under different conditions should remain close to their respective set points. In other words, as the network transitions from standard conditions to degraded conditions, an SNN with stronger homeostasis is expected to exhibit smaller changes in firing rates, reflected by lower values of the HM_m and HM_{std} metrics.

Table 1 compares firing rate changes in the host SNN with and without DWAM across various degraded conditions. DWAM consistently reduces both metrics, except in the SAN-SRM model under 8-bit Loihi weights. These results support DWAM's effectiveness in embedding biologically inspired homeostatic regulation into SNNs.

4.2 Continuous Control with DWAM

The continuous control tasks include HalfCheetah-v3 and Ant-v3, which vary in complexity: HalfCheetah has a 17D observation and 6D action space, while Ant uses 110D and 8D, respectively. This diversity enables a comprehensive evaluation of DWAM in continuous control. In both tasks, the objective is to control a six-joint half-mechanical cheetah (HalfCheetah) or a quadruped robot (Ant) to move forward for 1000 steps while maximizing velocity. As in the obstacle avoidance task, we tested under degraded conditions based on the baseline environment, including degraded input (disturbing observations via "MIN", "MAX", and "GN") and weight uncertainty (same as in obstacle avoidance). Detailed explanations of these disturbance methods can be found in Supplementary Note 6.

Reward The reward comparison between the host SNN and the host SNN integrated with DWAM under degraded conditions for the HalfCheetah-v3 and Ant-v3 tasks is shown in Table 2 and 3. The comparison was conducted using both the LIF and SRM neuron models. Across all degraded conditions, the cumulative rewards of the host SNN show clear improvements after integrating DWAM. Specifically, SAN-DWAM consistently outperforms SAN, with the most noticeable gains observed under challenging input perturbations based on the LIF model. Similarly, BDETT-DWAM achieves higher rewards than BDETT, particularly under severe weight degradation using the SRM model. These findings, combined with the earlier results from the obstacle avoidance task, further validate the generalization capability of DWAM. It not only enhances performance in specific tasks but also demonstrates robustness across diverse task domains.

Homeostasis Metrics The impact of various degraded conditions on the firing rate changes of the host SNN and

	MIN				MAX				GN			
	LIF		SRM		LIF		SRM		LIF		SRM	
Name	Reward	HM_m/HM_{std}	Reward	HM_m/HM_{std}	Reward	HM_m/HM_{std}	Reward	HM_m/HM_{std}	Reward	HM_m/HM_{std}	Reward	HM_m/HM_{std}
PopSAN	9993	0.035/0.036	10354	0.029/0.027	10251	0.028/0.027	10511	0.030/0.027	4050	0.085/0.073	3641	0.095/0.084
PopSAN-DWAM	**10155**	**0.032/0.034**	**10413**	**0.026/0.025**	**10306**	**0.027/0.026**	**10639**	**0.027/0.025**	**4139**	**0.083/0.072**	**3705**	**0.093/0.083**
BDETT	9906	0.020/**0.027**	11050	0.017/0.018	9756	0.023/0.028	10723	0.018/0.018	3425	**0.057**/0.066	3701	0.086/0.071
BDETT-DWAM	**10003**	**0.019/0.027**	**11149**	**0.016/0.017**	**9864**	**0.021/0.027**	**10868**	**0.017/0.017**	**3498**	**0.057/0.065**	**4037**	**0.076/0.061**
	8-bit Loihi weight				**GN weight**				**30% Zero weight**			
	LIF		SRM		LIF		SRM		LIF		SRM	
Name	Reward	HM_m/HM_{std}	Reward	HM_m/HM_{std}	Reward	HM_m/HM_{std}	Reward	HM_m/HM_{std}	Reward	HM_m/HM_{std}	Reward	HM_m/HM_{std}
PopSAN	10576	**0.003/0.003**	10793	**0.003**/0.003	7158	**0.055**/0.046	9671	0.023/0.021	4467	0.105/0.088	7255	0.066/0.055
PopSAN-DWAM	**10651**	**0.003/0.003**	**10807**	**0.003/0.002**	**7194**	**0.055/0.045**	**9882**	**0.021/0.019**	**4845**	**0.103/0.087**	**7522**	**0.063/0.053**
BDETT	10253	**0.002/0.002**	11278	0.005/**0.006**	8885	0.017/**0.017**	10691	0.015/0.013	1584	0.091/0.097	8167	0.049/**0.038**
BDETT-DWAM	**10327**	**0.002/0.002**	**11414**	**0.004/0.006**	**8962**	**0.016/0.017**	**11048**	**0.014/0.010**	**1759**	**0.088/0.094**	**8219**	**0.047/0.038**

Table 2: Quantitative performance of the Half Cheetah-v3 task under degraded conditions, where higher reward indicates better performance, and lower HM_m and HM_{std} values reflect improved homeostasis.

	MIN				MAX				GN			
	LIF		SRM		LIF		SRM		LIF		SRM	
Name	Reward	HM_m/HM_{std}	Reward	HM_m/HM_{std}	Reward	HM_m/HM_{std}	Reward	HM_m/HM_{std}	Reward	HM_m/HM_{std}	Reward	HM_m/HM_{std}
PopSAN	3521	0.092/0.066	5687	0.057/0.060	4795	**0.079**/0.077	5430	0.051/0.049	2160	0.125/0.091	2109	0.093/**0.080**
PopSAN-DWAM	**3794**	**0.066/0.060**	**5709**	**0.055/0.059**	**4900**	**0.079/0.76**	**5581**	**0.048/0.047**	**2541**	**0.105/0.087**	**2153**	**0.092/0.080**
BDETT	4186	**0.039/0.061**	4275	0.058/0.052	3638	**0.049/0.071**	4510	0.064/0.063	2182	**0.070**/0.093	2275	0.090/0.073
BDETT-DWAM	**4214**	**0.039/0.061**	**4388**	**0.056/0.050**	**3691**	**0.049/0.071**	**4516**	**0.063/0.062**	**2230**	**0.069/0.092**	**2517**	**0.080/0.062**
	8-bit Loihi weight				**GN weight**				**30% Zero weight**			
	LIF		SRM		LIF		SRM		LIF		SRM	
Name	Reward	HM_m/HM_{std}	Reward	HM_m/HM_{std}	Reward	HM_m/HM_{std}	Reward	HM_m/HM_{std}	Reward	HM_m/HM_{std}	Reward	HM_m/HM_{std}
PopSAN	5904	0.008/0.011	6044	0.007/0.007	1324	0.185/0.113	5580	0.025/0.021	1580	0.124/0.108	4091	0.078/0.063
PopSAN-DWAM	**5948**	**0.007/0.010**	**6050**	**0.006/0.005**	**1519**	**0.145/0.097**	**5627**	**0.021/0.019**	**1873**	**0.122/0.102**	**4219**	**0.077/0.062**
BDETT	4732	**0.003**/0.004	5732	0.008/0.010	3626	0.023/**0.028**	4939	0.040/0.035	1937	0.055/0.072	4949	0.040/0.035
BDETT-DWAM	**4774**	**0.003/0.003**	**5822**	**0.007/0.009**	**3637**	**0.022/0.028**	**5558**	**0.017/0.015**	**2157**	**0.053/0.071**	**5030**	**0.037/0.033**

Table 3: Quantitative performance of the Ant-v3 task under degraded conditions, where higher reward indicates better performance, and lower HM_m and HM_{std} values reflect improved homeostasis.

the host SNN integrated with DWAM in the HalfCheetah-v3 and Ant-v3 tasks are shown in Table 2 and 3, respectively. In all degraded conditions, the homeostasis metrics of the host SNN showed consistent reductions following the incorporation of DWAM.

These results further confirm that the proposed DWAM is an effective method for introducing biologically-inspired homeostatic mechanisms into SNNs. By minimizing deviations in neuronal firing rates, it stabilizes network performance, even under challenging conditions.

5 Conclusion

In this paper, we proposed the DWAM as a biologically-inspired approach to integrating homeostatic mechanisms into SNNs. Drawing on the principles of the BCM theory, DWAM enables SNNs to dynamically regulate synaptic strength, maintaining network stability across varying levels of neuronal activity. We evaluated the proposed method across multiple tasks and under various degradation conditions. The experimental results demonstrated that DWAM not only enhances the performance of SNNs lacking homeostatic mechanisms in challenging scenarios but also seamlessly integrates with existing homeostatic methods, improving the performance of host SNNs already equipped with such features. This method broadens the scope of SNN design, offering a novel perspective for enhancing network robustness and adaptability in a biologically plausible manner. Nevertheless, the interplay and joint effects of multiple homeostatic mechanisms within SNNs remain poorly understood. If such mechanisms could not only coexist but also complement each other as they do in biological systems, more effective and resilient forms of homeostasis might be achieved — a promising direction for future research.

Acknowledgements

The study has been supported by National Key Research and Development Program of China (No.2022ZD0210500).

References

Benuskova, L.; Diamond, M. E.; and Ebner, F. F. 1994. Dynamic synaptic modification threshold: computational model of experience-dependent plasticity in adult rat barrel cortex. *Proceedings of the National Academy of Sciences*.

Bienenstock, E. L.; Cooper, L. N.; and Munro, P. W. 1982. Theory for the development of neuron selectivity: orientation specificity and binocular interaction in visual cortex. *Journal of Neuroscience*.

Brockman, G. 2016. OpenAI Gym. *arXiv preprint arXiv:1606.01540*.

Desai, N. S. 2003. Homeostatic plasticity in the CNS: synaptic and intrinsic forms. *Journal of Physiology-Paris*.

Ding, J.; Dong, B.; Heide, F.; Ding, Y.; Zhou, Y.; Yin, B.; and Yang, X. 2022. Biologically inspired dynamic thresholds for spiking neural networks. *Advances in Neural Information Processing Systems*.

Fujimoto, S.; Hoof, H.; and Meger, D. 2018. Addressing function approximation error in actor-critic methods. In *International Conference on Machine Learning*.

Gerstner, W. 1995. Time structure of the activity in neural network models. *Physical Review E*.

Gerstner, W.; and Kistler, W. M. 2002. *Spiking neuron models: Single neurons, populations, plasticity*. Cambridge university press.

Gupta, A.; and Saurabh, S. 2024. Unsupervised learning in a ternary SNN using STDP. *IEEE Journal of the Electron Devices Society*.

Hao, W.; Andolina, I. M.; Wang, W.; and Zhang, Z. 2021. Biologically inspired visual computing: the state of the art. *Frontiers of Computer Science*.

Hao, Y.; Huang, X.; Dong, M.; and Xu, B. 2020. A biologically plausible supervised learning method for spiking neural networks using the symmetric STDP rule. *Neural Networks*.

Keck, T.; Hübener, M.; and Bonhoeffer, T. 2017. Interactions between synaptic homeostatic mechanisms: an attempt to reconcile BCM theory, synaptic scaling, and changing excitation/inhibition balance. *Current opinion in neurobiology*.

Kheradpisheh, S. R.; Ganjtabesh, M.; Thorpe, S. J.; and Masquelier, T. 2018. STDP-based spiking deep convolutional neural networks for object recognition. *Neural Networks*.

Kim, T.; Hu, S.; Kim, J.; Kwak, J. Y.; Park, J.; Lee, S.; Kim, I.; Park, J.-K.; and Jeong, Y. 2021. Spiking neural network (snn) with memristor synapses having non-linear weight update. *Frontiers in computational neuroscience*.

Maass, W. 1997. Networks of spiking neurons: the third generation of neural network models. *Neural networks*.

Marder, E.; and Goaillard, J.-M. 2006. Variability, compensation and homeostasis in neuron and network function. *Nature Reviews Neuroscience*.

Marder, E.; and Prinz, A. A. 2002. Modeling stability in neuron and network function: the role of activity in homeostasis. *Bioessays*.

Mease, R. A.; Famulare, M.; Gjorgjieva, J.; Moody, W. J.; and Fairhall, A. L. 2013. Emergence of adaptive computation by single neurons in the developing cortex. *Journal of Neuroscience*.

Meng, Y.; Jin, Y.; and Yin, J. 2011. Modeling activity-dependent plasticity in BCM spiking neural networks with application to human behavior recognition. *IEEE transactions on neural networks*.

Olshausen, B. A.; and Field, D. J. 1996. Emergence of simple-cell receptive field properties by learning a sparse code for natural images. *Nature*.

O'Leary, T.; Williams, A. H.; Franci, A.; and Marder, E. 2014. Cell types, network homeostasis, and pathological compensation from a biologically plausible ion channel expression model. *Neuron*.

Pan, W.; Zhao, F.; Zeng, Y.; and Han, B. 2023. Adaptive structure evolution and biologically plausible synaptic plasticity for recurrent spiking neural networks. *Scientific Reports*.

Roy, K.; Jaiswal, A.; and Panda, P. 2019. Towards spike-based machine intelligence with neuromorphic computing. *Nature*.

Stringer, C.; Pachitariu, M.; Steinmetz, N.; Carandini, M.; and Harris, K. D. 2019. High-dimensional geometry of population responses in visual cortex. *Nature*.

Tang, G.; Kumar, N.; and Michmizos, K. P. 2020. Reinforcement co-learning of deep and spiking neural networks for energy-efficient mapless navigation with neuromorphic hardware. *arXiv preprint arXiv:2003.01157*.

Tang, G.; Kumar, N.; Yoo, R.; and Michmizos, K. P. 2020. Deep Reinforcement Learning with Population-Coded Spiking Neural Network for Continuous Control. *arXiv preprint arXiv:2010.09635*.

Turrigiano, G. G.; and Nelson, S. B. 2004. Homeostatic plasticity in the developing nervous system. *Nature reviews neuroscience*.

Wang, Y.; Dong, B.; Zhang, Y.; Zhou, Y.; Mei, H.; Wei, Z.; and Yang, X. 2023. Event-enhanced multi-modal spiking neural network for dynamic obstacle avoidance. In *Proceedings of the 31st ACM International Conference on Multimedia*.

Wang, Y.; Mei, H.; Bao, Q.; Wei, Z.; Shou, M. Z.; Li, H.; Dong, B.; and Yang, X. 2024. Apprenticeship-inspired elegance: synergistic knowledge distillation empowers spiking neural networks for efficient single-eye emotion recognition. *arXiv preprint arXiv:2407.09521*.

Xu, M.; Liu, F.; and Pei, J. 2022. Endowing spiking neural networks with homeostatic adaptivity for APS-DVS bimodal scenarios. In *Companion Publication of the 2022 International Conference on Multimodal Interaction*.

Zhang, J.; Dong, B.; Zhang, H.; Ding, J.; Heide, F.; Yin, B.; and Yang, X. 2022. Spiking transformers for event-based single object tracking. In *Proceedings of the IEEE/CVF conference on Computer Vision and Pattern Recognition*.

Zhang, J.; Zhang, M.; Wang, Y.; Liu, Q.; Yin, B.; Li, H.; and Yang, X. 2025. Spiking neural networks with adaptive membrane time constant for event-based tracking. *IEEE Transactions on Image Processing*.